Biomaterials 32 (2011) 9888–9898

Contents lists available at SciVerse ScienceDirect

Biomaterials

journal homepage: www.elsevier.com/locate/biomaterials

Low molecular weight protamine-functionalized nanoparticles for drug delivery to the brain after intranasal administration

Huimin Xia[a,1], Xiaoling Gao[b,1], Guangzhi Gu[a], Zhongyang Liu[a], Ni Zeng[c], Quanyin Hu[a], Qingxiang Song[b], Lei Yao[b], Zhiqing Pang[a], Xinguo Jiang[a], Jun Chen[a,*], Hongzhuan Chen[b,*]

[a] Key Laboratory of Smart Drug Delivery, Ministry of Education & PLA, School of Pharmacy, Fudan University, Lane 826, Zhangheng Road, Shanghai 201203, PR China
[b] Department of Pharmacology, Institute of Medical Sciences, Shanghai Jiaotong University School of Medicine, 280 South Chongqing Road, Shanghai 200025, PR China
[c] Department of Pharmaceutical Science, School of Pharmacy, Shenyang Pharmaceutical University, Shenyang, Liaoning 110016, PR China

ARTICLE INFO

Article history:
Received 21 August 2011
Accepted 1 September 2011
Available online 19 September 2011

Keywords:
Brain targeting
Low molecular weight protamine
Nanoparticles
Intranasal administration

ABSTRACT

The development of new strategies for enhancing drug delivery to the brain is of great importance in diagnostics and therapeutics of central nervous diseases. Low-molecular-weight protamine (LMWP) as a cell-penetrating peptide possesses distinct advantages including high cell translocation potency, absence of toxicity of peptide itself, and the feasibility as an efficient carrier for delivering therapeutics. Therefore, it was hypothesized that brain delivery of nanoparticles conjugated with LMWP should be efficiently enhanced following intranasal administration. LMWP was functionalized to the surface of PEG-PLA nanoparticles (NP) via a maleimide-mediated covalent binding procedure. Important parameters such as particle size distribution, zeta potential and surface content were determined, which confirmed the conjugation of LMWP to the surface of nanoparticle. Using 16HBE14o- cells as the cell model, LMWP-NP was found to exhibit significantly enhanced cellular accumulation than that of unmodified NP via both lipid raft-mediated endocytosis and direct translocation processes without causing observable cytotoxic effects. Following intranasal administration of coumarin-6-loaded LMWP−NP, the $AUC_{0-8\ h}$ of the fluorescent probe detected in the rat cerebrum, cerebellum, olfactory tract and olfactory bulb was found to be 2.03, 2.55, 2.68 and 2.82 folds, respectively, compared to that of coumarin carried by NP. Brain distribution analysis suggested LMWP-NP after intranasal administration could be delivered to the central nervous system along both the olfactory and trigeminal nerves pathways. The findings clearly indicated that the brain delivery of nanoparticles could be greatly facilitated by LMWP and the LMWP-functionalized nanoparticles appears as a effective and safe carrier for nose-to-brain drug delivery in potential diagnostic and therapeutic applications.

1. Introduction

The presence of the blood–brain barrier (BBB), which limits the distribution of systemically administered therapeutics to the central nervous system (CNS), poses a major challenge to drug development efforts to combat the CNS disorders [1]. Therefore, the development of effective strategies to enhance drug delivery to the brain is of great interest in both clinical and pharmaceutical fields. Nowadays there are some potential approaches for brain drug delivery in either the invasive or non-invasive manners. The invasive approaches consist of a temporary disruption of BBB allowing the entry of a drug into the CNS, or of a direct drug delivery by means of intraventricular or intracerebral administration [2], while the non-invasive ones are made possible by the systemic application of colloidal drug carriers undergoing a receptor or adsorptive-mediated transcytosis mechanism [3], or by bypassing the BBB via intranasal delivery [4].

Intranasal delivery is considered as a promising alternative which could bypass the blood–brain barrier to rapidly deliver therapeutic agents to the brain for treating CNS disorders [5–12]. It provides the advantages including a large surface area for absorption, rapid achievement of target drug levels, avoidance of first pass metabolism and improvement of drug bioavailability; furthermore, this delivery route is needleless, maximizing patient comfort and compliance. It has been demonstrated that part of the therapeutics could be delivered directly to the CNS within minutes along both the olfactory and trigeminal nerves [13–15]. However, the total

* Corresponding authors. Tel.: +86 21 51980066; fax: +86 21 51980069.
E-mail addresses: chenjun@fudan.edu.cn (J. Chen), hongzhuan_chen@hotmail.com (H.Z. Chen).
[1] Authors contributed equally.

0142-9612/$ – see front matter © 2011 Elsevier Ltd. All rights reserved.
doi:10.1016/j.biomaterials.2011.09.004

amount of drugs reported to access the brain was still low, especially for nasally applied biotech drugs such as peptides, proteins and DNA, which were poorly absorbed and highly susceptible to the harmful environment of the nasal cavity [16–18].

The application of nanoparticles offers an improvement to nose-to-brain drug delivery since they are able to protect the encapsulated drug from biological and/or chemical degradation, and extracellular transport by P-gp efflux proteins [19]. Despite these advances, the amount of nose-to-brain drug delivery mediated by nanoparticles is still not satisfied. A key mechanism to enhance nasal adsorption of nanoparticles is to improve their transmucosal transport, which may be facilitated by the surface modification with bioactive peptides such as cell-penetrating peptides (CPPs).

CPPs are relatively short peptides of 5–40 amino acids in length that derived from natural sources such as animal toxin [20] or from synthetically designed constructs. They hold remarkable capacity for membrane translocation and gaining access to the cell interior. CPPs such as TAT have been previously reported as efficient drug carriers to deliver many kinds of cargoes to the brain through the BBB [21–23]. Among the CPPs, low molecular weight protamine (LMWP) (CVSRRRRRRGGRRRR), which possess high arginine content and carry significant sequence similarity to that of the virus-derived TAT peptide, was found to be as potent as TAT in mediating cellular translocation of the attached cargos. In addition, unlike other cationic proteins/peptides, LMWPs were neither antigenic [24] nor mutagenic [25], and exhibited a much-reduced toxicity and thus an improved safety profile over protamine. Besides these advantages, while other CPPs must be chemically synthesized, LMWP can be produced in mass quantities direct from native protamine with limited processing time and cost [26]. Therefore, LMWP could be practically employed as an effective, safe and economical carrier for drug delivery. Indeed, it has been reported that LMWP has been utilized in facilitating anticancer [27,28] and percutaneous drug delivery [29]. As CPPs have been employed for the delivery of a wide variety of cargo including small molecules, nucleic acids, antibodies and nanoparticles, and the highly efficient translocation capacity of CPPs has been observed in a variety of cell lines [30–33]. In this study, we speculated that LWMP might serve as an effective and safe CPP for facilitating the nose-to-brain delivery of drug-loaded nanoparticles.

In order to justify this hypothesis, LWMP was functionalized to the surface of poly (ethyleneglycol)-poly (lactic acid) (PEG-PLA) nanoparticles, and brain delivery property of the developed nanoparticles was extensively studied following intranasal delivery. The nanoparticles (NP) were prepared with an emulsion/evaporation method, and functionalized with thiolated LMWP by taking advantage of the thiol group coupling activity of maleimide. The physicochemical characteristics of the nanoparticles were investigated by means of morphology, particle size, zeta potential and the surface elemental analysis. Coumarin-6 was used as a probe to study the brain-targeting efficiency of this system. Cellular association of LWMP-NP was evaluated on 16HBE14o- cells and compared with that of the unmodified ones. Endocytosis inhibition experiments were performed to clarify the mechanism of cellular association of LMWP-NP. *In vitro* cytotoxicity of LMWP-NP were analyzed by a cell counting kit-8 (CCK-8) assay and compared with that of NP to evaluate its safety as drug delivery carrier. Finally, brain biodistribution of the fluorescent marker associated to LMWP-NP following intranasal administration were qualitatively and quantitatively analyzed and compared with that of coumarin-6 carried by the unmodified NP. The possible pathway that LMWP-NP travels from the nasal cavity to the brain following intranasal administration was also discussed.

2. Experimental

2.1. Materials and animals

LMWP were synthesized by ChinaPeptides Co., Ltd (Shanghai, China). Methoxy poly(ethylene glycol) $_{3000}$-poly(lactic acid) $_{34000}$ (MePEG-PLA) and maleimide-poly (ethylene glycol) $_{3400}$-poly(lactic acid) $_{34000}$ (Male-PEG-PLA) were kindly provided by East China University of Science and Technology. Coumarin-6, coumarin-7 and DiR (1, 1′- dioctadecyl- 3,3,3′,3′- tetramethyl indotricarbocyanine Iodide) were purchased from Sigma–Aldrich (St. Louis, MO, USA). DAPI (4,6-diamidino-2-phenylindole) was obtained from Molecular Probes (Eugene, OR, USA), and cell counting kit-8 (CCK-8) from Dojindo Laboratories (Japan). Cell culture media, DMEM nutrient mix F12, certified fetal bovine serum (FBS), penicillin/streptomycin stock solutions and 0.25% Trypsin-EDTA were purchased from Invitrogen Co., USA. All the other chemicals were of analytical grades and used without further purification.

Male Sprague–Dawley rats weighing 200 ± 20 g were obtained from BK Lab Animal Ltd. (Shanghai, China) and maintained at 25 ± 1 °C with free access to food and water. The protocol of animal experiments was approved by the Animal Experimentation Ethics Committee of Fudan University.

2.2. Nanoparticles preparation and characterization

2.2.1. Preparation of NP and LMWP-NP

Unmodified nanoparticles (NP) loaded with coumarin-6 were prepared through an emulsion/solvent evaporation technique [34]. In brief, MePEG-PLA (22.5 mg), Male-PEG-PLA (2.5 mg) and 0.1% (w/w) of coumarin-6 were dissolved in 1 ml dichloromethane, and then added into a 2 ml of 1% sodium cholate aqueous solution with the mixture emulsified by sonication (280 w, 30 s) on ice using probe sonicator (Ningbo Scientz Biotechnology Co. Ltd., China). The O/W emulsion was diluted into an 8 ml of 0.5% sodium cholate aqueous solution under magnetic stirring for 5 min. After evaporating dichloromethane with a ZX-98 rotavapor (Shanghai Institute of Organic Chemistry, China) at 30 °C, the obtained nanoparticles were concentrated by centrifugation at 15000 rpm for 45 min using a TJ-25 centrifuge (Beckman Counter, USA). With the supernatant discarded, the nanoparticles were resuspended in double-distilled water, subjected to a 1.5 × 20 cm sepharose CL-4B column (Pharmacia Biotech, Inc., Sweden) and eluted with 0.01 M HEPES buffer (pH 7.0) to remove the unentrapped coumarin-6. Nanoparticles modified with LMWP (LMWP-NP) were prepared via a maleimide-thiol coupling reaction at room temperature for 8 h as described previously. The products were then eluted with 0.01 M HEPES buffer (pH 7.0) through the 1.5 × 20 cm sepharose CL-4B column to remove the unconjugated peptide.

2.2.2. Morphology, particle size, zeta potential and X-ray photo electron spectroscopy (XPS)

The morphological examination of nanoparticles was performed by transmission electron microscopy (TEM) (H-600, Hitachi, Japan) following negative stain with sodium phosphotungstate solution. Particle size and zeta potential were determined using Nicomp™ 380 XLS Zeta Potential/Particle Sizer (PSS·Nicomp, USA).

To determine the surface composition of NP and LMWP-NP, the samples were lyophilized using an ALPHA 2-4 Freeze Dryer (0.070 Mbar Vakuum, −80 °C, Martin Christ, Germany) and subjected to XPS analysis. The determination was performed on a RBD upgraded PHI-5000C ESCA system (Perkin Elmer) and the data analysis was carried out by using the RBD AugerScan 3.21 software provided by RBD Enterprises.

2.2.3. In vitro release of coumarin-6 from NP and LMWP-NP

To evaluate if the fluorescence probe remained associated with the particles during a 24 h incubation period, the *in vitro* release of coumarin-6 from the nanoparticles was investigated under sinking condition. Coumarin-6-loaded NP and LMWP-NP were incubated at 37 °C in pH 4 and pH 7.4 PBS, at a coumarin-6 concentration of 50 ng/ml with a shaking rate at 100 rpm [35]. One milliliter of nanoparticle samples was withdrawn at 0 min, 5 min, 15 min, 30 min, 1 h, 2 h, 4 h, 8 h, 12 h, 24 h ($n = 6$). Periodic samples were subject to centrifuged at 15000 rpm for 45 min and the supernatant was further diluted with methanol and analyzed for the released coumarin-6 by HPLC assay. The cumulative release percentage (CR %) of coumarin-6 from nanoparticles was calculated using the following equation [36,37]:

$$\mathrm{CR}(\%) = \frac{\text{amount of coumarin-6 in the supernatant}}{\text{total amount of coumarin-6}} \times 100\%$$

2.3. Cellular association of coumarin-6-labeled NP and LMWP-NP in 16HBE14o- cells

2.3.1. Cell culture

16HBE14o- cells, human bronchial epithelial cell line, were maintained in DMEM nutrient mix F12 containing L-glutamine, 15 mM HEPES, 10% fetal bovine

serum, 100 U/ml penicillin and 100 μg/ml streptomycin under standardized conditions (95% relative humidity, 5% CO_2, 37 °C).

2.3.2. Cellular association of LWMP-NP in 16HBE14o- cells

Qualitative analysis of cellular association of LWMP-NP in 16HBE14o- cells was performed via fluorescent microscopy. In brief, 16HBE14o- cells were plated on a 96-well plate at the density of 5×10^3 cells/well. Twenty-four hours later, the cells were incubated with coumarin-6-loaded NP and LMWP-NP (300 μg/ml nanoparticles in HBSS, containing coumarin-6 200 ng/ml) for 15, 30 min, 1, 2 and 3 h at 37 °C, respectively. After that, the cells were washed three times with PBS, fixed with 4% formaldehyde for 20 min. After that, the nuclei of the cells were stained with 100 ng/ml DAPI for 10 min. Finally, the cells were washed three times with PBS, and observed under a fluorescent microscope (Olympus, Japan).

Quantitative analysis of cellular association of coumarin-6-loaded NP and LMWP-NP was conducted using a high content analysis system as described previously [38,39]. 16HBE14o- cells were plated on a 96-well plate at the density of 5×10^3 cells/well. Twenty four hours later, the cells were incubated with nanoparticles (3.75–600 μg/ml) for 1 h at 4 °C and 37 °C, respectively. After that, the cells were washed with PBS and fixed with 3.7% formaldehyde solution for 10 min. After stained with 10 μg/ml Hochest 33258 at room temperature, away from light for 10 min, the cells was finally washed for three times and detected under a KineticScan® HCS Reader (version 3.1, Cellomics Inc., Pittsburgh, PA, USA). To determine if the cellular association of nanoparticle was time dependent, the cells were incubated with the nanoparticles (200 μg/ml) at 37 °C for 15, 30 min, 1, 2 and 3 h, respectively, and the quantitative analysis was performed as above.

Endocytosis inhibition experiments were performed to investigate the cellular internalization mechanism for LMWP-NP in 16HBE14o- cells. LMWP (1 mg/ml) and other endocytic inhibitors (10 μg/ml chlorpromazine, 4 μg/ml colchicines, 10 μg/ml cyto-D, 5 μg/ml BFA, 5 μg/ml filipin, 10 mM NaN_3, 50 mM deoxyglucose, 2.5 mM methyl-β-cyclodextrin (M-β-CD), 200 nM monensin, 20 μM nocodazole) were preincubated with the cells for 30 min, respectively, before their addition and incubation with NP or LMWP-NP (90 μg/ml, 1 h, 37 °C). Quantitative analysis of the cellular association of nanoparticles following the inhibitor treatments was performed as mentioned above and compared with that of the non-inhibited control.

2.3.3. In vitro cytotoxicity of LMWP-NP on 16HBE14o- cells

To evaluate the cytotoxicity of LMWP-NP, cell viability following LMWP-NP treatment was measured with CCK-8 assay according to the manufacturer's instruction [40]. 16HBE14o- cells were seeded into 96-well plates at the density of 5×10^3 cells/well and incubated at 37 °C, 5% CO_2 for 24 h to allow cell attachment. NP and LMWP-NP of 0.01–2.0 mg/ml in the culture media were incubated with the cells for 3 h at 37 °C. Cell viability was expressed as percentage of absorbance in comparison with that of the control, which was comprised of cells treated with the culture medium.

2.4. In vivo distribution of LMWP-NP following intranasal administration

2.4.1. Qualitative studies

For qualitative studies, near infrared dye DiR was employed as a probe to minimize the autofluorecence background [41]. The DiR-loaded NP or LMWP-NP was prepared using the method described above. For intranasal administration, rats were anesthetized with 10% hydral (0.3 ml/100 g, i.p.), and fixed in a supine position. The preparations were given at the openings of the nostrils using a polyethylene 10 (PE 10) tube attached to a microliter syringe (0.5 mg DiR/kg, 10 μl/nostril), allowing the rats to sniff the drop into the nasal cavity. The procedure lasted about 5 min. One hour after the administration, the animals were euthanized with the brains, hearts, livers, spleens, lungs and kidneys harvested and subjected to imaging under a Maestro *in vivo* imaging system (CRI, MA).

In order to study the distribution profile of LMWP-NP in the brain, coumarin-6 was used as the fluorescent probe and coumarin-6-labeled NP and LMWP-NP were given nasally to two groups of rats ($n = 3$), respectively. Each animal received a total amount of nanoparticles containing coumarin-6 20 μg in 20 μl (10 μl/nostril). One hour later, the animals were anesthetized with 10% hydral and then fixed by heart perfusion with 100 ml saline and 200 ml of 4% paraformaldehyde sequentially. After that, the brains and trigeminal nerves were removed, fixed in 4% paraformaldehyde for 24 h, dehydrated with sucrose solution, and subjected to OCT (Sakura, Torrance, CA, USA) embedding and frozen section. Finally, the sections were transferred to microscope slides, counterstained with 4′, 6-diamidino-2-phenylindole (DAPI) (100 ng/ml) and observed under a fluorescence microscope (Olympus IX71)

2.4.2. Quantitative studies

Thirty-six rats were divided into two groups: one was dosed with the unconjugated NP, and the other with LMWP-NP. Each animal received a total of 20 μl nanoparticles (10 μl each nostril) containing 5 μg coumarin-6. At each time points (0.25, 0.5, 1, 2, 4 and 8 h) following the administration, the animals were euthanized and decapitated, and blood was collected into the tube with heparin. Followed by a quick washing with cold saline, the brain were collected and excised in the order of the cerebrum, cerebellum, olfactory tract and olfactory bulb.

To prepare the samples for analysis, the organ samples were homogenized with 3-fold volumes of distilled water. Then 10 μl of coumarin-7 (10 ng/ml, internal standard) and 1 ml of n-hexane was added to 200 μl of the homogenate to extract the fluorescent dye from the samples. After intensely vortexed for 5 min, the mixture was subjected to centrifuge at 12000 rpm for 5 min. The supernatant was collected and evaporated under a stream of nitrogen at 40 °C. The residue was dissolved in 50 μl of methanol. Afterward, the mixture was vortexed and subsequently centrifuged at 12000 rpm for 10 min with the supernatant subjected to liquid chromatography- tandem mass spectrometry (LC-MS/MS) analysis. The whole blood samples were homogenized without the addition of water and treated in the same manner. An Agilent 1100 system consisting of a G1312A quaternary pump, a G1379A vacuum degasser, a G1316A thermostatted column oven (Agilent, Waldbronn, Germany) and a HTS PAL autosampler (CTC Analytics , Switzerland) was used. Mass spectrometric detection was performed on an API 3000 triple quadrupole instrument (Applied Biosystems, Toronto, Canada) in multiple reaction monitoring (MRM) mode. A TurboIonSpray ionization (ESI) interface in positive ionization mode was used. Data processing was performed with Analyst 1.4.1 software package (Applied Biosystems). The chromatographic separation was achieved on a Gemini C18 column (100 mm × 2.0 mm i.d., 3.0 μm, Phenomenex, Torrance, CA, USA). A mixture of methanol–2 mM ammonium acetate–formic acid (90:10:0.1, v/v/v) was used as mobile phase at a flow rate of 0.35 mL/min. The temperature of column and autosampler were maintained at 40 °C and 4 °C respectively. The chromatographic run time of each sample was 3.5 min. The mass spectrometer was operated using ESI source in the positive ion detection. Quantitation was done using multiple reaction monitoring (MRM) mode to monitor protonated precursor→product ion transition of m/z 351.3→307.1 for Coumarin 6, 334.1→290.1 for Coumarin 7. Turbo spray voltage (IS) was set at 5000 V. Source temperature was maintained at 500 °C. Entrance potential (EP) was set at 10 V. Nitrogen was used as nebulizing gas (8 l/min) and curtain gas (8 l/min). For collision activated dissociation (CAD), nitrogen was employed as the collision gas at a pressure of 4 l/min. The compound dependent parameters like declustering potential (DP), focusing potential (FP), collision energy (CE) and cell exit potential (CXP) were optimized at 100, 200, 50 and 20 V for Coumarin-6, 80, 220, 50 and 15 V for Coumarin-7 respectively. Quadrupole 1 and quadrupole 3 were maintained at unit resolution. Dwell time set was 200 ms for all the analytes. All the concentration data were dose-normalized and plotted as plasma drug concentration-time curves. Drug and Statistics software for Windows (DAS ver 2.1.1) was utilized to calculate the pharmacokinetic parameters.

2.5. Statistical analysis

All the data were expressed as mean ± standard deviation (SD) and comparison between different groups was performed by one-way ANOVA followed by Bonferroni tests. Statistical significance was defined as $p < 0.05$.

3. Results

3.1. Preparation and characterization of NP and LMWP-NP

Nanoparticles were prepared with an emulsion/solvent evaporation method. Representative transmission electron micrographs illustrated that NP (Fig. 1A) and LMWP-NP (Fig. 1B) were generally spherical with a uniform distribution. The particle size, zeta potential and polydispersity index (PI) of NPs were presented in Table 1. The results demonstrated that volume-based diameter of NP was between 80 nm and 90 nm. After the conjugation with LMWP, the average diameter increased slightly. The polydispersity of all the formulations also showed quite narrow size distribution (PI < 0.3). The zeta potential of NP was negative (−20.50 ± 0.43 mV), while that of LMWP-NP was positive (2.42 ± 0.81 mV). XPS analysis showed that the elemental composition percentage of nitrogen on the surface of unconjugated NPs and in the mixed copolymers (22.5 mg MePEG-PLA and 2.5 mg Male-PEG-PLA) were undetectable, while that on the surface of LMWP-NP was 1.15% (Table 2).

3.2. In vitro release of coumarin-6 from NP and LMWP-NP

The results of the *in vitro* release study conducted in pH 4.0 and pH 7.4 PBS, which represented the pH in the endo-lysosomal compartment and physiologic pH respectively, at 37 °C showed that no more than 5% of coumarin-6 was released from NP and LMWP–NP after a 24 h incubation period (Fig. 1C).

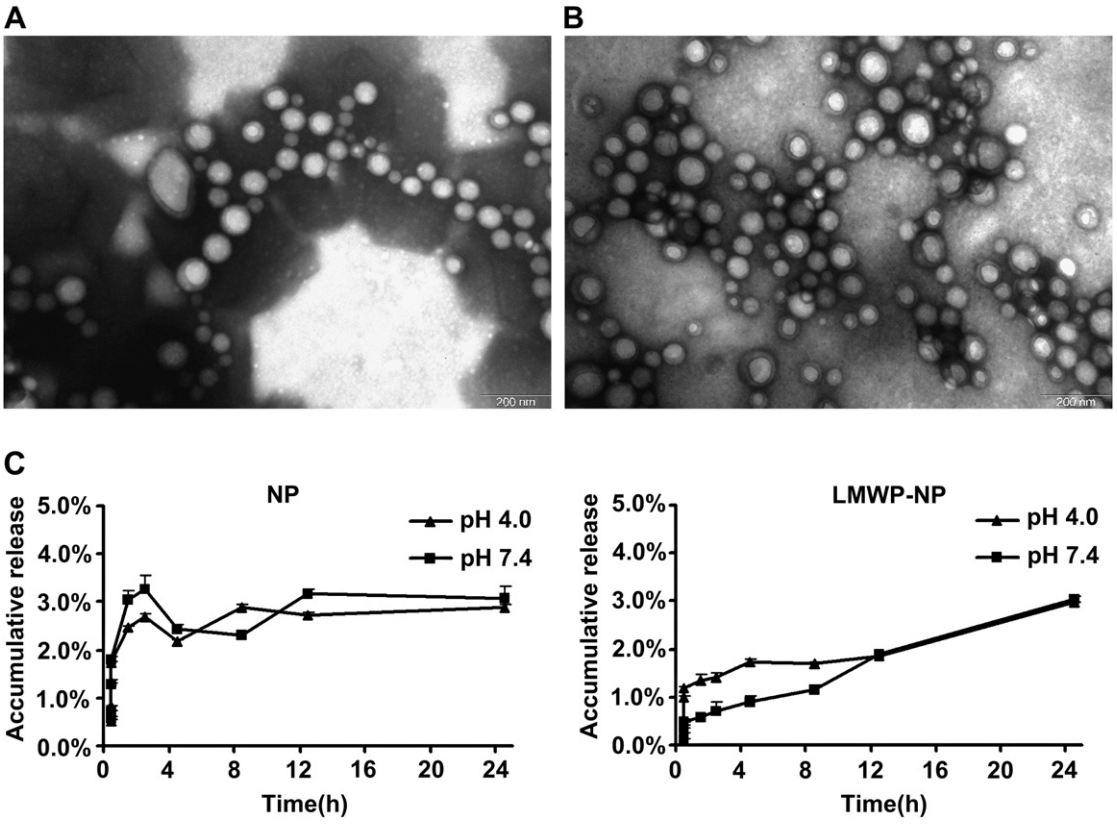

Fig. 1. Characterization of NP and LMWP-NP. (A) Transmission electron micrographs of NP; (B) Transmission electron micrographs of LMWP-NP. Bar, 200 nm; (C) *In vitro* release of coumarin-6 from NP and LMWP-NP in 0.1 M PBS buffer of pH = 7.4 and 4.0.

3.3. Cellular association of NP and LWMP-NP in 16HBE14o- cells

Qualitative analysis under the fluorescent microscope demonstrated that the cellular association of the fluorescent probe-loaded nanoparticles increased in a time-dependent manner (Fig. 2). And a significantly higher accumulation of LMWP–NP in the cells was found when compared with that of NP.

Quantitative analysis confirmed the time-dependent cellular association of NP and LMWP-NP in 16HBE14o- cells (Fig. 3A). Besides, the cellular association of both LMWP-NP and NP was also found to be temperature and concentration-dependant (Fig. 3B).

At each time and concentration point, the cellular association of LMWP-NP was higher than that of NP (about 1.58 times higher than that of NP after 3 h incubation at the concentration of 300 μg/ml and reached 3.69 times of that of NP at 600 μg/ml after 1 h incubation at 37 °C).

Endocytosis inhibition experiments showed that the cellular association of both NP and LMWP-NP were inhibited by M-β-CD (Fig. 4), but not affected by other inhibitors including chlorpromazine, colchicines, cyto-D, BFA, filipin, NaN_3, deoxyglucose, monensin and nocodazole. Besides, a competitive effect was observed between LWMP and LWMP-NP but not between LWMP and NP (Fig. 4A).

Table 1
Physical characterization of NP and LWMP-NP (Data represent mean ± SD, $n = 3$).

Formulation	Particle size (nm)	Polydispersity index (PI)	Zeta potential (mV)
NP	85.37 ± 3.39	0.12 ± 0.016	−20.50 ± 0.43
LMWP-NP	110.77 ± 5.61	0.27 ± 0.11	2.42 ± 0.81

3.4. Cytotoxicity of NP and LMWP-NP on 16HBE14o- cells

To evaluate the safety of LMWP-NP system, CCK-8 method was used to determine cell viability after LMWP-NP treatment. The result exhibited that under our experimental condition, the cell viability was over 80% following both NP and LWMP-NP treatments and no significant difference in cell viability was observed between the LMWP-NP and NP treatments (Fig. 5).

3.5. In vivo distribution of NP and LMWP-NP following nasal administration

3.5.1. Qualitative studies

One hour after nasal administration, various organs of rats were harvested for optical images. An obvious stronger fluorescence of DiR signal was detected in the brains of rats administered with DiR-loaded LMWP-NP when compared with that in those treated with DiR-loaded NP (Fig. 6A). Besides, the nanoparticles were found mainly distributed in the liver, spleen and kidney (Fig. 6B).

Fluorescence microscopy examination revealed that coumarin-6 was widely distributed in the brain and observed in the cortex, hippocampi, ventricle, thalamencephalon and olfactory bulb

Table 2
X-ray photo electron spectroscopy (XPS) analysis of the mixed copolymers, NP and LMWP-NP.

XPS elemental ratio (%)	Copolymers	NP	LMWP-NP
C	75.33	70.18	71.18
O	24.67	29.82	27.67
N	–	–	1.15

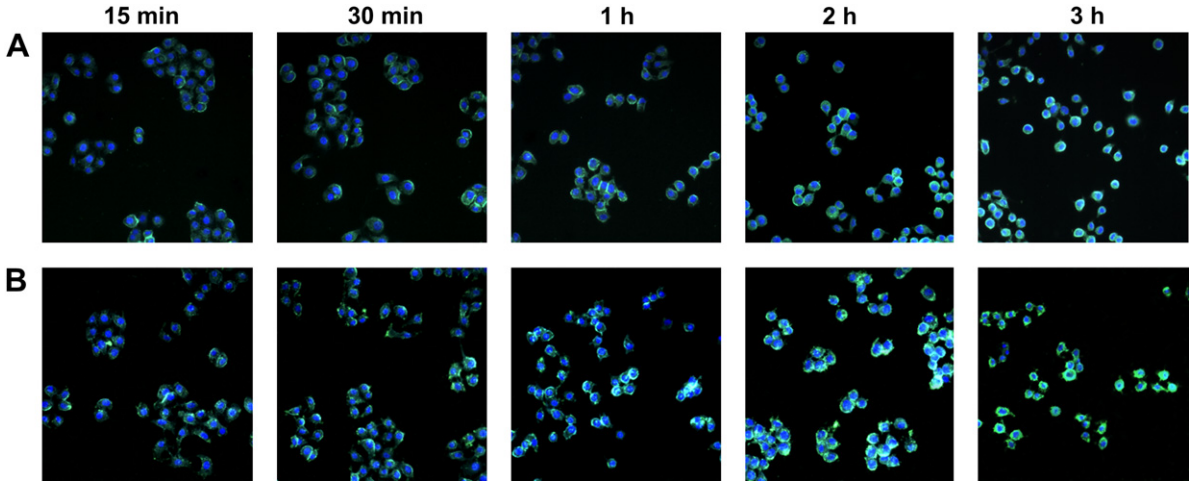

Fig. 2. Cellular association of (A) NP and (B) LMWP-NP at 37 °C after an incubation for 15, 30 min, 1, 2 and 3 h, respectively. Green, coumarin-6-loaded nanoparticles; Blue, cell nuclei stained with DAPI. (For interpretation of the references to colour in this figure legend, the reader is referred to the web version of this article.)

(Fig. 7). The fluorescence signal observed in the animals treated with LMWP-NP (Fig. 7B) was much higher than that in NP-treated ones (Fig. 7A). Besides, the signal of the fluorescent marker was also observed in the trigeminal nerves (Fig. 7).

3.5.2. Quantitative studies

The pharmacokinetic data showed that after intranasal administration, the highest blood coumarin-6 concentration was achieved at 1 h after dosing for both unconjugated NP and LMWP-NP (Fig. 8). $AUC_{0-8\ h}$ of coumarin carried by LWMP-NP was about 1.6 folds compared with that of coumarin associated to the unmodified NP. The blood clearance $t_{1/2}$ were 2.599 h and 2.733 h for NP and LMWP-NP, respectively (Table 3).

Brain uptake of coumarin-6 after intranasal administration of LMWP-NP, increased significantly when compared with that following nasal application of unconjugated NP ($AUC_{0-8\ h}$ increased by 103%, 155%, 168% and 182% for cerebrum, cerebellum, olfactory tract and olfactory bulb, respectively) (Fig. 9). The pharmacokinetic parameters were showed in Table 3. The ratio of $AUC_{0-8\ h,\ Brain\ tissue}$ to $AUC_{0-8\ h,\ Blood}$ of coumarin incorporated in LWMP-NP was found to be much higher than that of coumarin associated to the unmodified NP.

4. Discussion

The blood–brain barrier (BBB) limits the distribution of therapeutics to the central nervous system (CNS). Intranasal delivery provides a non-invasive and convenient method that rapidly targets therapeutics to the CNS, bypassing the BBB and minimizing systemic exposure. The use of nanoparticles may offer an improvement to nose-to-brain drug delivery since they are able to protect the encapsulated drug from biological and/or chemical degradation, and extracellular transport by efflux proteins such as P-gp. Surface modification of the nanoparticles provides an effective strategy in improving brain-targeting delivery. Recent researches have witnessed the capability of CPPs in facilitating therapeutic molecules through the BBB and into the brain following intravenous administration [42–45]. Among these CPPs, LMWP offers distinct advantages, including high cell translocation potency, neither antigenic nor mutagenic and relative ease and low costs of production. In this contribution, LMWP was firstly reported to be functionalized to the surface of PEG-PLA nanoparticles to improve its brain delivery following intranasal administration.

The functionalized nanoparticles (LMWP-NP) was constructed via a maleimide-mediated covalent binding procedure. As shown in Table 1, the particle size of the LMWP-NP was larger than that of the unconjugated NP. Particle size is an important property that is associated with the mucosal transport, and particles smaller than 100 nm, in general, have higher transport [46]. Thus, the nanoparticles obtained with diameters of approximately 100 nm in this study can facilitate the nasal absorption and further uptake into CNS. Furthermore, it has been previously reported that a small diameter potentially allows nanoparticles to be transported transcellularly through olfactory neurons to the brain via various

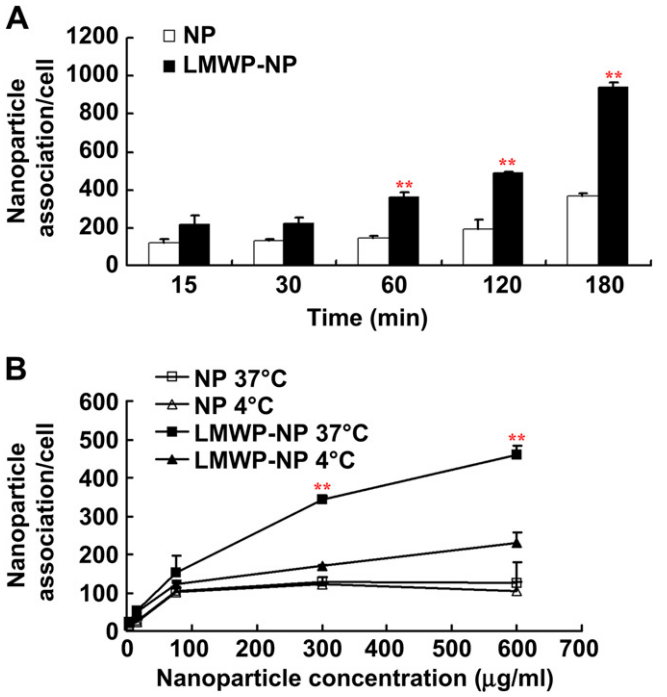

Fig. 3. Cellular association of coumarin-6-loaded nanoparticles on 16HBE14o- cells (A) The cells were incubated with LMWP-NP and NP (200 μg/mL) at 37 °C for 15, 30, 60, 120 and 180 min, respectively. (B) The cells were incubated with LMWP-NP and NP (3.75–600 μg/ml) for 1 h at 37 and 4 °C, respectively. $^{*}p < 0.05$, $^{**}p < 0.01$ significantly different with that of NP at the same concentration and same temperature.

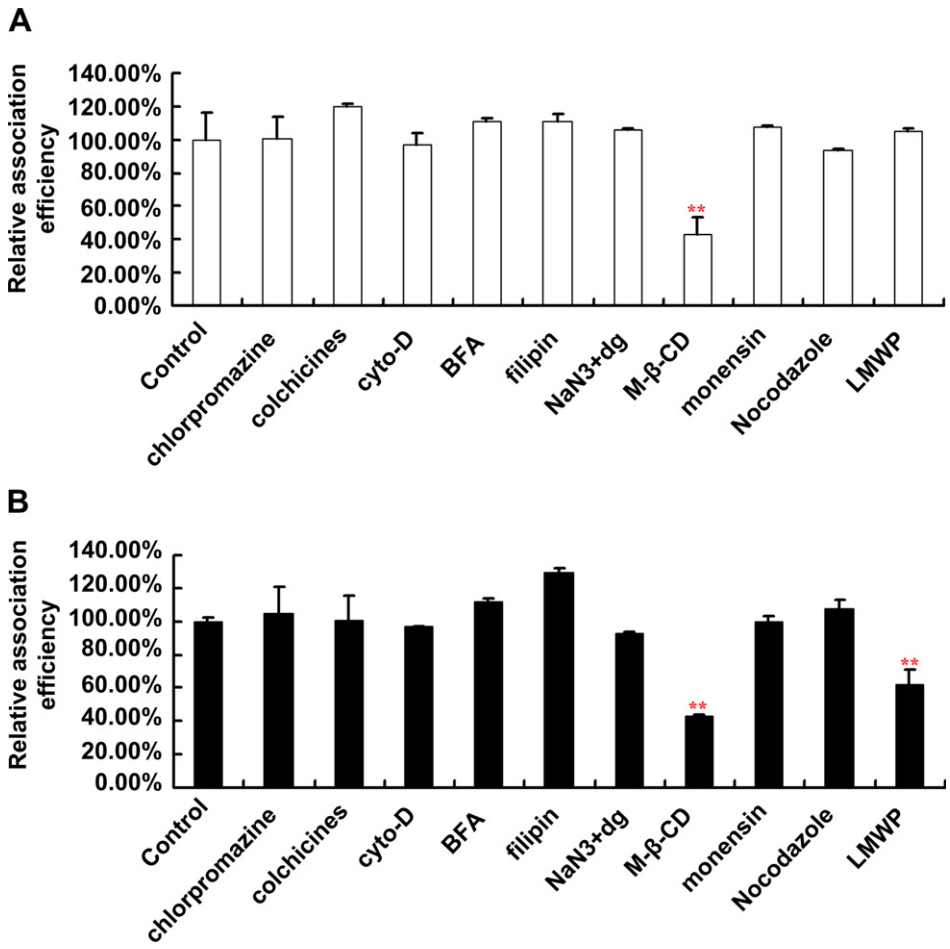

Fig. 4. Cellular association of coumarin-6-loaded (A) NP or (B) LMWP-NP in the presence of different endocytosis inhibitors. Data represent mean ± SD, $n = 3$, $^{*}p < 0.05$, $^{**}p < 0.01$ significantly different with that of the non-inhibited control.

endocytic pathways of sustentacular or neuronal cells in the olfactory membrane [11,13,47,48]. Therefore, these findings indicate that the size of the prepared NP and LMWP-NP were regarded as favorable for intranasal brain delivery.

The unmodified NP presented a negative surface charge, while LMWP-NP showed a slightly positive one. We believed that this was resulted from the surface decoration with LMWP, a positively charged peptide. The modification of LMWP on the surface of NP was further verified by the XPS analysis, which showed that the elemental composition percentage of nitrogen on the surface of unconjugated NPs was undetectable, similar with that in the mixed copolymers (22.5 mg MePEG-PLA and 2.5 mg Male-PEG-PLA), while that on the surface of LMWP-NP was 1.15%. The increased signal of nitrogen was ascribed to LWMP. These results together strongly confirmed the decoration of LWMP on the nanoparticle surface.

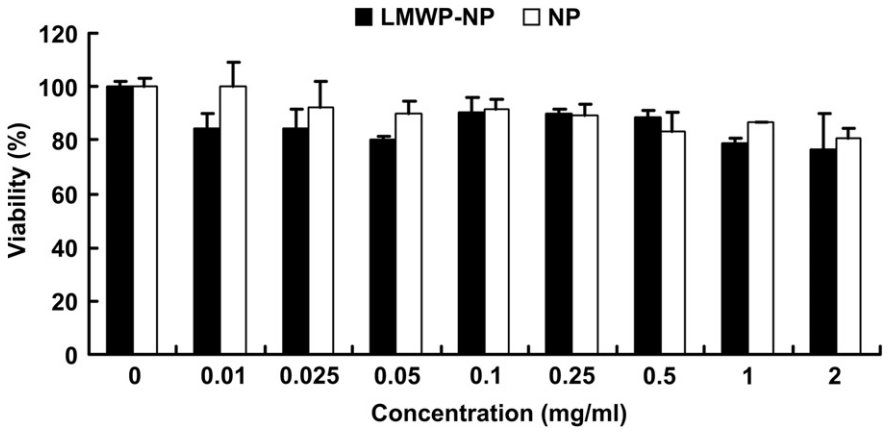

Fig. 5. *In vitro* cytotoxicity of NP and LMWP-NP on 16HBE14o- at the nanoparticles concentrations ranging from 0 to 2 mg/ml ($n = 3$).

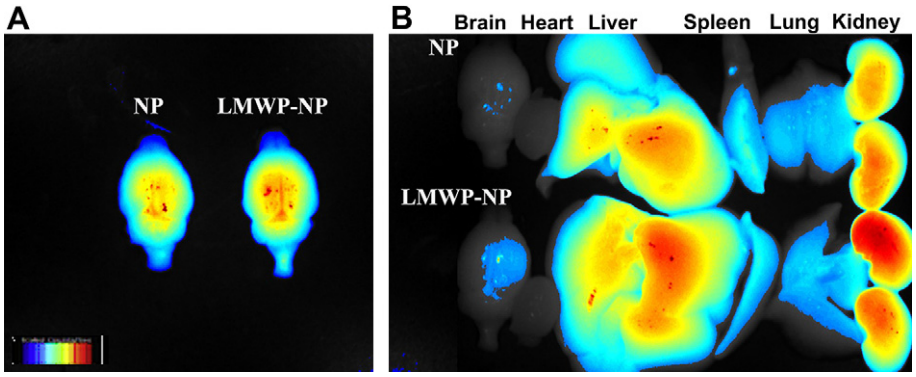

Fig. 6. *In vivo* distribution of LMWP-NP following intranasal administration. Representative optical images taken 1 h after dose under a dedicated imaging system designed for small animals imaging. Distribution in the (A) brain and (B) main organs.

Consistent with previous researches [49], the results of *in vitro* release experiment showed that no more than 5% of coumarin-6 was released from NP and LMWP-NP after a 24 h incubation period, which clearly suggested that almost all the fluorescent tracer retained associated with the nanoparticles in the experimental period and indicated that the fluorescence signal detected in the cell or tissue samples was mainly attributed to the coumarin-6 encapsulated into the nanoparticles. Therefore, coumarin-6 was considered as a proper fluorescent probe for the evaluation of both *in vitro* and *in vivo* behavior of nanoparticles. Actually, coumarin-6 has been widely applied for allowing the visualization of brain uptake of nanoparticles in many researches [35,50–53].

In vitro cellular association of NP and LMWP-NP was performed on 16HBE14o- cells, a human bronchial epithelial cell line. It has been reported that there was little difference between the cultured nasal and bronchial epithelial cells with respect to either morphology or ciliary activity [54]. In the present study, 16HBE14o- cells were chosen as a cell model to study the nasal cellular association of the developed formulations. As shown in Figs. 2 and 3, LMWP-NP showed significant higher cellular association than the unmodified NP, indicating that LMWP-NP exhibited better cellular internalization property.

In order to figure out the cellular interaction mechanism of LMWP-NP, endocytosis inhibition experiments were performed in this study. As mentioned previously, understanding the cellular interaction mechanism of CPPs-cargoes constitutes an essential piece of the puzzle for their therapeutic developments. Although, it remains difficult to establish a general scheme for its cellular interaction mechanism, there is a consensus that the first contacts between the CPPs and the cell surface take place through electrostatic interactions with proteoglycans, and that the cellular uptake pathway is driven by several parameters including (i) the nature and secondary structure of the CPP, (ii) its ability to interact with cell surface and membrane lipid components, (iii) the nature, type and active concentration of the cargo and (iv) the cell type and cell cycle status [55–60]. Therefore, it is significant to study the specific association and uptake mechanism for LMWP-NP in 16HBE14o- cells.

The time-, temperature- and concentration- dependant cellular association of the nanoparticles suggested a process of active endocytosis. As cellular endocytosis includes macropinocytosis, clathrin-mediated endocytosis, and caveloae/lipid raft-mediated endocytosis [30], in this study, to characterize the endocytosis mechanism involved in the cellular uptake of LMWP-NP, cellular association experiments were performed in the presence of various endocytosis inhibitors. The results indicated that the cellular association of both NP and LMWP-NP were inhibited by M-β-CD (Fig. 4), which is a cyclic oligomer of glucopyranoside that inhibits cholesterol-dependent endocytic processes by reversibly extracting the steroid out of the plasma membrane. M-β-CD is regularly used to determine whether endocytosis is dependent on the integrity of lipid rafs [61]. The inhibition of M-β-CD on the internalization of NP and LWMP-NP, suggesting that cellular import was mediated by lipid raft-mediated endocytosis. In addition, internalization into cells still occurred, although reduced, at low temperature (4 °C), suggesting that besides endocytosis, at least another internalization mechanism exists in the cellular internalization of LWMP-NP, which we speculated was ascribed to the energy-independent direct translocation effect of LWMP [30]. Therefore, the mechanisms described so far should be shared between two general pathways: endocytosis and direct translocation.

A competitive effect was observed between LWMP and LWMP-NP: when the cells were preincubated with excess free LMWP for

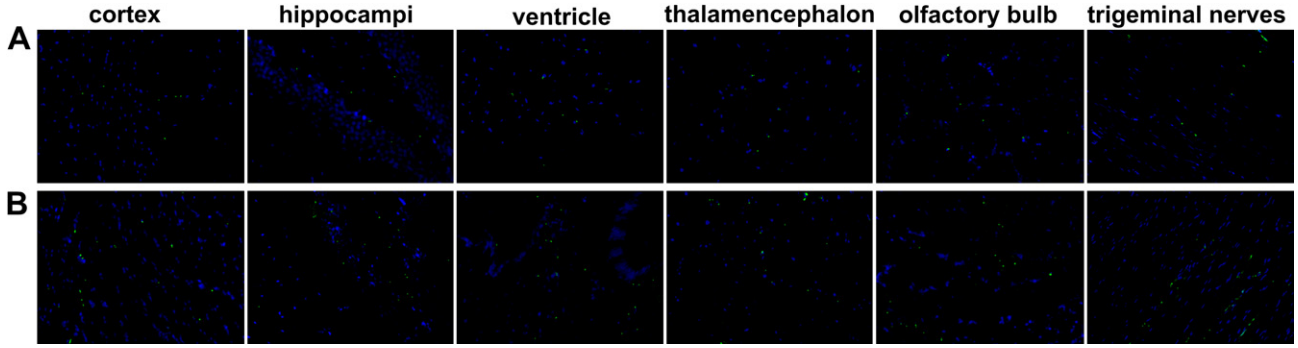

Fig. 7. Distribution of NPs in the brains of rats 1 h after administration with coumarin-6-loaded (A) NP and (B) LMWP-NP, respectively. Green: coumarin-6-loaded nanoparticles; Blue: cell nuclei stained with DAPI. (For interpretation of the references to colour in this figure legend, the reader is referred to the web version of this article.)

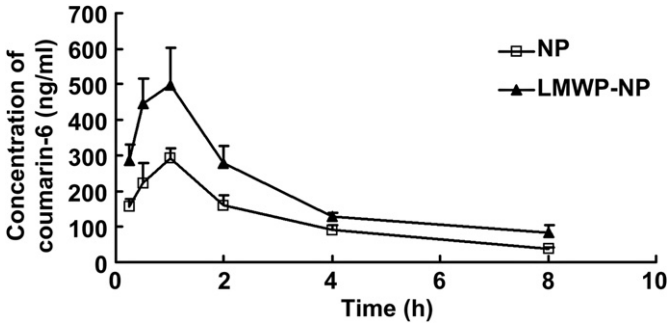

Fig. 8. Blood concentration-time profiles of coumarin-6 following intranasal administration of coumarin-6 loaded LMWP-NP and NP. Data represented the mean ± S.D. $n = 3$.

30 min, the cellular association of LMWP-NP was significantly reduced (Fig. 4B). This result demonstrated that the enhanced association of LMWP-NP compared to unmodified NP was contributed by LMWP. We inferred that the excess free LMWP reduced the binding sites available for LMWP-NP, thus specifically inhibited the association of LMWP-NP in 16HBE14o- cells. The exact mechanisms for the cellular internalization of the LMWP-cargoes need to be further identified.

The property of cationized proteins to efficiently penetrate cells raises the question of its potential toxicity. Therefore, to evaluate the cytotoxicity of LMWP-NP, cell viability following LMWP-NP treatment was measured with a CCK-8 assay. PLA polymers are generally accepted as being of low cytotoxicity with good biocompatibility and biodegradability. Moreover, both PEG and PLA are materials approved by FDA [62,63]. Thus, unconjugated PLA-NP was regarded as the safety control. LMWP peptides actually possess significantly reduced antigenicity, mutagenicity, and complement-activating activity, as well as fewer other cationic, polymer-associated, hemodynamic/hematologic toxic effects than does the parent protamine, a U.S. FDA-approved clinical drug [24,26,27]. Therefore, our LMWP-functionalized PEG-PLA NP has a good safety theoretically. This hypothesis was justified by the cytotoxicity data which showed that under our experimental condition, the cell viability was over 80% following both the NP and LWMP-NP treatments and no significant difference was observed between the two nanoparticles treatments at any of the given concentrations (Fig. 5). Accordingly, LMWP-NP was considered as a promising drug carrier without observable cytotoxic effects.

Biodistribution analysis under the *in vivo* imaging system showed that after intranasal dosing, the nanoparticles were distributed mainly into the liver, spleen and kidney (Fig. 6B), which might be attributed to their non-specific capture by the mononuclear phagocyte system. After modification, more LMWP-NP was found distributed in the brain as well as in the liver and kidney. This was believed to be contributed by the non-tissue-specific cellular translocation property of CPPs. This property of CPPs raised the importance of topical applications, among which intranasal administration offers the highest potential as it might facilitate direct drug delivery to the CNS along both the olfactory and trigeminal nerve pathways [13–15]. Although a small increase of LMWP-NP was also detected in other organs, compared with conventional oral drug administration and intravenous administration, the relative drug delivery into the brain was believe to be much enhanced.

For quantitatively evaluating the brain uptake of LMWP-NP and NP, coumarin-6 was incorporated into the nanoparticles, and the blood and brain concentrations of the fluorescent marker were detected with a LC-MS/MS detection method. The proposed LC-MS/MS method under multiple-reaction monitoring (MRM) mode provided much higher sensitivity compared to other reported procedures. It demonstrated excellent performance in terms of selectivity, ruggedness and efficiency. To our knowledge, none of the authors evaluated the efficacy of MS/MS as an LC detector for the analysis of coumarin-6. As showed in Fig. 8, an initial rapid and extensive increase in blood coumarin concentration occurred during the beginning 1 h post administration, and after 8 h, the concentration of coumarin-6 still can be detected. Besides, the blood clearance $t_{1/2}$ of LMWP-NP is slightly longer than that of NP, suggesting the conjugation of an adequate amount of LMWP on the surface of NP did not impair the long-circulation characteristic of PEG.

The brain distribution data showed that LMWP modification facilitated the uptake of fluorescence tracer embedded in the nanoparticles into the cerebrum, cerebellum, olfactory tract and olfactory bulb, with a huge increase in $AUC_{0-8\ h}$ and C_{max} at the time point of 1 h (Table 3). These results were believed to be brought from the fact that the conjugated LMWP contributed to higher transmucosal transport and more accumulation of LMWP-NP in the CNS. In order to determine whether there is a direct nose-to-brain transport, the drug targeting efficiency defined as AUC_{brain}/AUC_{blood} ratios was calculated after intranasal administration and listed in Table 3. As shown in Table 3, although LMWP modification facilitated the absorption of the fluorescent tracer into both the brain and the circulation, the AUC_{brain}/AUC_{blood} values of LMWP-NP after intranasal administration were much higher than those obtained for NP, indicating that LMWP functionalization might also facilitate direct brain delivery of the nanoparticles. Therefore, LMWP-NP might serve as promising carriers with elevated brain-targeting capacity.

The brain uptake of intact coumarin-6, compared with that after intranasal administration of unmodified NP, was significantly increased following nasal application of LWMP-NP ($AUC_{0-8\ h}$ 2.03, 2.55, 2.68 and 2.82 folds for cerebrum, cerebellum, olfactory tract

Table 3
Pharmacokinetic parameters of coumarin-6 following an intranasal administration of coumarin-loaded LMWP-NP and NP.

Formulation	Tissue	C_{max} (pg/ml or pg/g)	T_{max} (h)	AUC_{0-8h} (pg h/ml or pg h/g)	AUC_{brain}/AUC_{blood}
LMWP-NP	Blood	497.439	1	1589.411	–
	OB	1038.467	1	3538.815	2.226
	OT	825.462	1	2782.732	1.751
	CR	1053.090	1	5133.735	3.230
	CL	1312.124	1	4352.37	2.738
NP	Blood	294.181	1	928.240	–
	OB	395.922	1	1251.410	1.348
	OT	287.945	1	1039.343	1.120
	CR	493.721	1	2529.757	2.725
	CL	531.726	1	1706.949	1.839

OB, olfactory bulb; OT, olfactory tract; CR, cerebrum; CL, cerebellum.

and olfactory bulb, respectively) (Fig. 9), which indicated that the LMWP functionalization could elevate the amount of nanoparticles gaining access to CNS, therefore enhance the absorption of the incorporated chemicals into the brain. Besides, the fluorescent probe showed a uniform distribution in the CNS (cerebrum, cerebellum, olfactory tract and olfactory bulb), which suggested that beside the well-known olfactory pathway which mainly contribute to drug delivery from the nasal mucosa to the forebrain, there may

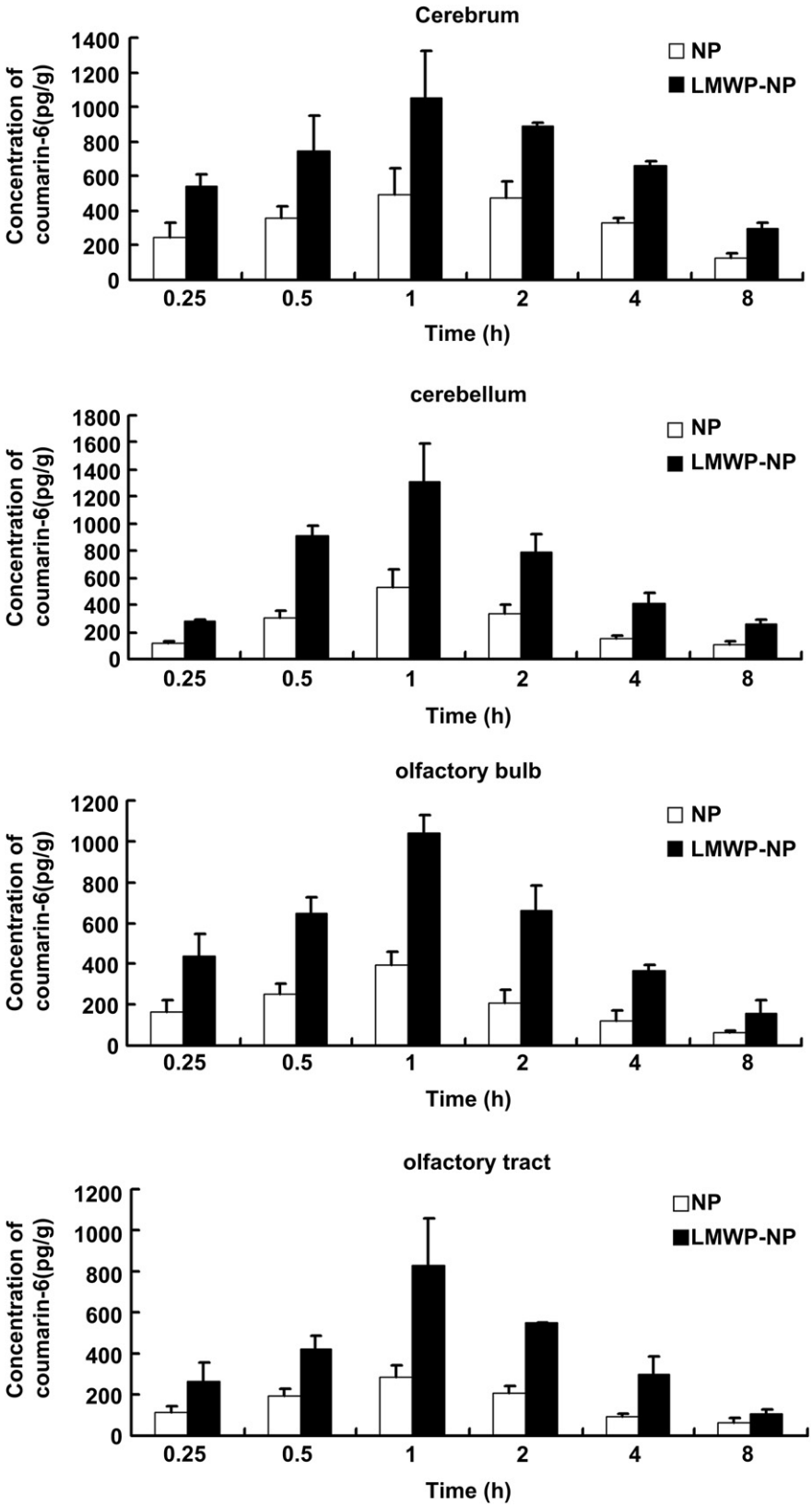

Fig. 9. Brain biodistribution of coumarin-6 following intranasal administration of coumarin-6-loaded LMWP-NP and NP in the cerebrum, cerebellum, olfactory bulb and olfactory tract.

exist other ways for delivery NP and LMWP-NP to the brain after intranasal administration. As shown by fluorescent microscopy analysis, strong fluorescent signal of the nanoparticles was also observed in the trigeminal nerves (Fig. 7), suggesting that LMWP-NP might also be directly delivered to the CNS along the trigeminal nerves pathway as suggested in previous researches [13–15]. It has been pointed out that following intranasal administration, the therapeutic agents could enter the trigeminal nerve and trigeminal neural pathway at three points from the nasal cavity: choana, middle nasal concha, and maxillary sinus [64], and then transport drug to the brainstem beginning at the entry through the pons and through the rest of the hindbrain [65]. A portion of the trigeminal nerve that passes through the cribriform plate might also contribute to delivery of drug from the nasal mucosa to the forebrain [13]. Therefore, it is highly speculated that following intranasal administration, besides the circulation transport, LWMP-NP might also travel from the nasal cavity to the brain via both the olfactory pathway and the trigeminal neural one.

5. Conclusion

The present study developed a new strategy of a nanoparticulate DDS decorated with LMWP for enhancing brain delivery following intranasal administration. LMWP was functionalized to the surface of PEG-PLA nanoparticles via a maleimide-mediated covalent binding technique. The conjugation was confirmed by zeta potential determination and XPS. The resulted LMWP-NP was observed to be uniformly spherical in shape with a particle size of 110.77 $\pm$ 5.61 nm and zeta potential of 2.42 $\pm$ 0.81 mV. Cellular experiments showed that LMWP-NP exhibited significantly enhanced cellular accumulation than that of unmodified NP via both lipid raft-mediated endocytosis and direct translocation processes without causing observable cytotoxicity. Following intranasal administration of coumarin-6-loaded LMWP-NP, the amount of the fluorescent probe detected in the rat cerebrum, cerebellum, olfactory tract and olfactory bulb was found to be much higher than that of coumarin carried by NP. Brain distribution analysis indicated that after intranasal administration LMWP-NP could be delivered to the central nervous system along both the olfactory and trigeminal nerves pathways. The technique described here might offer a safe and effective non-invasive delivery system for nose-to-brain drug delivery in potential diagnostic and therapeutic application of central nervous diseases.

Acknowledgments

This work was supported by National Key Basic Research Program (2007CB935800, 2010CB529800), National Natural Science Foundation of China (30801439, 81072592, 30801442) and Grants from Shanghai Science and Technology Committee Rising-Star Program (10QA1404100).

References

[1] Shadab AP, Zeenat I, Syed MAZ, Sushma T, Divya V, Gaurav KJ, et al. CNS drug delivery systems: novel approaches. Recent Pat Drug Deliv Formul 2009;3:71–89.
[2] Tosi G, Costantino L, Rivasi F, Ruozi B, Leo E, Vergoni AV, et al. Targeting the central nervous system: in vivo experiments with peptide-derivatized nanoparticles loaded with loperamide and rhodamine-123. J Control Release 2007;122:1–9.
[3] Kreuter J. Nanoparticulate system for brain delivery of drugs. Adv Drug Deliv Rev 2001;47:65–81.
[4] Dhuria SV, Hanson LR, Frey 2nd WH. Intranasal delivery to the central nervous system: mechanisms and experimental considerations. J Pharm Sci 2010;99:1654–73.
[5] Hanson LR, Frey 2nd WH. Intranasal delivery bypasses the blood-brain barrier to target therapeutic agents to the central nervous system and treat neurodegenerative disease. BMC Neurosci 2008;9:S5.
[6] Hanson L, Roeytenberg A, Martinez PM, Coppes VG, Sweet DC, Rao RJ, et al. Intranasal deferoxamine provides increased brain exposure and significant protection in rat ischemic stroke. J Pharmacol Exp Ther 2009;330:679–86.
[7] Hashizume R, Ozawa T, Gryaznov SM, Bollen AW, Lamborn KR, Frey 2nd WH, et al. New therapeutic approach for brain tumors: intranasal delivery of telomerase inhibitor GRN163. Neuro Oncol 2008;10:112–20.
[8] Liu XF, Fawcett JR, Hanson LR, Frey 2nd WH. The window of opportunity for treatment of focal cerebral ischemic damage with noninvasive intranasal insulin-like growth factor-I in rats. J Stroke CerebroVasc Dis 2004;13:16–23.
[9] Kissel T, Werner U. Nasal delivery of peptides: an in vitro cell culture model for the investigation of transport and metabolism in human nasal epithelium. J Control Release 1998;53:195–203.
[10] Frey 2nd WH. Bypassing the blood-brain barrier to delivery therapeutic agents to the brain and spinal cord. Drug Del Tech 2002;2:46–9.
[11] Dhanda DS, Frey 2nd WH, Leopold D, Kompella UB. Approaches for drug deposition in the human olfactory epithelium. Drug Del Tech 2005;5:64–72.
[12] Costantino HR, Illum L, Brandt G, Johnson PH, Quay SC. Intranasal delivery: physicochemical and therapeutic aspects. Int J Pharm 2007;337:1–24.
[13] Thorne RG, Pronk GJ, Padmanabhan V, Frey 2nd WH. Delivery of insulin-like growth factor-I to the rat brain and spinal cord along olfactory and trigeminal pathways following intranasal administration. Neuroscience 2004;127:481–96.
[14] Ross TM, Martinez PM, Renner JC, Thorne RG, Hanson LR, Frey 2nd WH. Intranasal administration of interferon beta bypasses the blood-brain barrier to target the central nervous system and cervical lymph nodes: a non-invasive treatment strategy for multiple sclerosis. J Neuroimmunol 2004;151:66–77.
[15] Thorne RG, Hanson LR, Ross TM, Tung D, Frey 2nd WH. Delivery of interferon-beta to the monkey nervous system following intranasal administration. Neuroscience 2008;152:785–97.
[16] Dufes C, Olivier JC, Gaillard F, Gaillard A, Couet W, Muller JM. Brain delivery of vasoactive intestinal peptide (VIP) following nasal administration to rats. Int J Pharm 2003;255:87–97.
[17] Frey WH, Liu J, Chen X, Thorne RG, Fawcett RG, Ala TA, et al. Delivery of 125I-NGF to the brain via the olfactory route. Drug Del 1997;4:87–92.
[18] Kim TW, Chung H, Kwon IC, Sung HC, Jeong SY. In vivo gene transfer to the mouse nasal cavity mucosa using a stable cationic lipid emulsion. Mol Cells 2000;10:142–7.
[19] Ali J, Ali M, Baboota S, Sahni JK, Ramassamy C, Dao L, et al. Potential of nanoparticulate drug delivery systems by intranasal administration. Curr Pharm Des 2010;16:1644–53.
[20] Ogris M, Carlisle RC, Bettinger T, Seymour LW. Melittin enables efficient vesicular escape and enhanced nuclear access of nonviral gene delivery vectors. J Biol Chem 2001;276:47550–5.
[21] Rao KS, Reddy MK, Horning JL, Labhasetwar V. TAT-conjugated nanoparticles for the CNS delivery of anti-HIV drugs. Biomaterials 2008;29:4429–38.
[22] Liu LH, Guo K, Lu J, Venkatraman SS, Luo D, Ng KC, et al. Biologically active core/shell nanoparticles self-assembled from cholesterol-terminated PEG-TAT for drug delivery across the blood-brain barrier. Biomaterials 2008;29:1509–17.
[23] Suk JS, Suh J, Choy K, Lai SK, Fu J, Hanes J. Gene delivery to differentiated neurotypic cells with RGD and HIV tat peptide functionalized polymeric nanoparticles. Biomaterials 2006;27:5143–50.
[24] Tsui B, Singh VJ, Liang JF, Yang VC. Reduced cross-reactivity towards anti-protamine antibodies of a low molecular weight protamine analogue. Thromb Res 2001;101:417–20.
[25] Liang JF, Zhen L, Chang LC, Yang VC. A less toxic heparin antagonist-low molecular weight protamine. Biochem (Mosc.) 2003;68:116–20.
[26] Lee LM, Chang LC, Wrobleski S, Wakefield TW, Yang VC. Low molecular weight protamine as nontoxic heparin/low molecular weight heparin antidote (III): preliminary in vivo evaluation of efficacy and toxicity using a canine model. AAPS PharmSci 2001;3:E19.
[27] Park YJ, Chang LC, Liang JF, Moon C, Chung CP, Yang VC. Nontoxic membrane translocation peptide from protamine, low molecular weight protamine (LMWP), for enhanced intracellular protein delivery: in vitro and in vivo study. FASEB J 2005;19:1555–7.
[28] Choi YS, Lee JY, Suh JS, Kwon YM, Lee SJ, Chung JK, et al. The systemic delivery of siRNAs by a cell penetrating peptide, low molecular weight protamine. Biomaterials 2010;31:1429–43.
[29] Huang YZ, Park YS, Moon C, David AE, Chung HS, Yang VC. Synthetic skin-permeable proteins enabling needleless immunization. Angew Chem Int Ed Enql 2010;49:2724–7.
[30] Fonseca SB, Pereira MP, Kelley SO. Recent advances in the use of cell-penetrating peptides for medical and biological applications. Adv Drug Deliv Rev 2009;61:953–64.
[31] Nam HY, Kim J, Kim S, Yockman JW, Kim SW, David A. Bull cell penetrating peptide conjugated bioreducible polymer for siRNA delivery. Biomaterials 2011;32:5213–22.
[32] Kim HY, Kim S, Youn H, Chung JK, Shin DH, Lee K. The cell penetrating ability of the proapoptotic peptide, KLAKLAKKLAKLAK fused to the N-terminal protein transduction domain of translationally controlled tumor protein, MIIYRDLISH. Biomaterials 2011;32:5262–8.

[33] Jiang QY, Lai LH, Shen J, Wang QQ, Xu FJ, Tang GP. Gene delivery to tumor cells by cationic polymeric nanovectors coupled to folic acid and the cell-penetrating peptide octaarginine. Biomaterials 2011;32:7253–62.
[34] Gao XL, Tao WX, Lu W, Zhang QZ, Zhang Y, Jiang XG, et al. Lectin-conjugated PEG-PLA nanoparticles: preparation and brain delivery after intranasal administration. Biomaterials 2006;27:3482–90.
[35] Lu W, Zhang Y, Tan YZ, Hu KL, Jiang XG, Fu SK. Cationic albumin-conjugated pegylated nanoparticles as novel drug carrier for brain delivery. J Control Release 2005;107:428–48.
[36] Wen ZY, Yan ZQ, Hu KL, Pang ZQ, Cheng XF, Guo LR, et al. Odorranalectin-conjugated nanoparticles: preparation, brain delivery and pharmacodynamic study on Parkinson's disease following intranasal administration. J Control Release 2011;151:131–8.
[37] Gao XL, Wu BX, Zhang QZ, Chen J, Zhu JH, Zhang WW, et al. Brain delivery of vasoactive intestinal peptide enhanced with the nanoparticles conjugated with wheat germ agglutinin following intranasal administration. J Control Release 2007;121:156–67.
[38] Gao XL, Wang T, Wu BX, Chen J, Chen JY, Yue Y, et al. Quantum dots for tracking cellular transport of lectin-functionalized nanoparticles. Biochem Biophys Res Commun 2008;377:35–40.
[39] Guo JW, Gao XL, Su LN, Xia HM, Gu GZ, Pang ZQ, et al. Aptamer-functionalized PEG-PLGA nanoparticles for enhanced anti-glioma drug delivery. Biomaterials 2011;32:8010–20.
[40] Salles II , Tucker AE, Voth DE, Ballard JD. Toxin-induced resistance in *bacillus anthracis* lethal toxin-treated macrophages. Proc Natl Acad Sci U S A 2003; 100:12426–31.
[41] Xin HL, Jiang XY, Gu JJ, Sha XY, Chen LC, Law K, et al. Angiopep-conjugated poly (ethyleneglycol)-co-poly (e-caprolactone) nanoparticles as dual-targeting drug delivery system for brain glioma. Biomaterials 2011;32:4293–305.
[42] Rousselle C, Smirnova M, Clair P, Lefauconnier JM, Chavanieu A, Calas B, et al. Enhanced delivery of doxorubicin into the brain via a peptide-vector-mediated strategy: saturation kinetics and specificity. J Pharmacol Exp Ther 2001;296:124–31.
[43] Rousselle C, Clair P, Smirnova M, Kolesnikov Y, Pasternak GW, Breton SG, et al. Improved brain uptake and pharmacological activity of dalargin using a peptide-vector-mediated strategy. J Pharmacol Exp Ther 2003;306:371–6.
[44] Rousselle C, Clair P, Temsamani J, Scherrmann JM. Improved brain delivery of benzyl penicillin with a peptide-vector-mediated strategy. J Drug Target 2002;10:309–15.
[45] Bourasset F, Cisternino S, Temsamani J, Scherrmann JM. Evidence for an active transport of morphine-6-beta-d-glucuronide but not P-glycoprotein-mediated at the blood-brain barrier. J Neurochem 2003;86:1564–7.
[46] Brooking J, Davis SS, Illum L. Transport of nanoparticles across the rat nasal mucosa. J Drug Target 2001;9:267–79.
[47] Mistry A, Stolnik S, Illum L. Nanoparticles for direct nose-to-brain delivery of drugs. Int J Pharm 2009;379:146–57.
[48] Thorne RG, Frey 2nd WH. Delivery of neurotrophic factors to the central nervous system: pharmacokinetic considerations. Clin Pharmacokinet 2001; 40:907–46.
[49] Zhang Y, Schlachetzki Y, Zhang YF, Boado RJ, Pardridge WM. Normalization of striatal tyrosine hydroxylase and reversal of motor impairment in experimental parkinsonism with intravenous nonviral gene therapy and a brain-specific promoter. Hum Gene Ther 2004;15:339–50.
[50] Li JW, Feng L, Fan L, Zha Y, Guo LR, Zhang QZ, et al. Targeting the brain with PEG-PLGA nanoparticles modified with phage-displayed peptides. Biomaterials 2011;32:4943–50.
[51] Hu KL, Li JW, Shen YH, Lu W, Gao XL, Zhang QZ, et al. Lactoferrin-conjugated PEG–PLA nanoparticles with improved brain delivery: in vitro and in vivo evaluations. J Control Release 2009;134:55–61.
[52] Yu DH, Lu Q, Xie J, Fang C, Chen HZ. Peptide-conjugated biodegradable nanoparticles as a carrier to target paclitaxel to tumor neovasculature. Biomaterials 2010;31:2278–92.
[53] Gan CW, Feng SS. Transferrin-conjugated nanoparticles of poly (lactide) -d-α-tocopheryl polyethylene glycol succinate diblock copolymer for targeted drug delivery across the blood-brain barrier. Biomaterials 2010;31:7748–57.
[54] Sapsforda RJ, Wells CW, Richman P, Daviesa RJ. Culture and comparison of human bronchial and nasal epithelial cells in vitro. Respir Med 1990;84: 303–12.
[55] Richard JP, Melikov K, Vives E, Ramos C, Verbeure B, Gait MJ, et al. Cell-penetrating peptides. A reevaluation of the mechanism of cellular uptake. J Biol Chem 2003;278:585–90.
[56] Nakase I, Niwa M, Takeuchi T, Sonomura K, Kawabata N, Koike Y, et al. Cellular uptake of arginine-rich peptides: roles for macropinocytosis and actin rearrangement. Mol Ther 2004;10:1011–22.
[57] Wadia JJ, Stan RV, Dowdy S. Transducible TAT-HA fusogenic peptide enhances escape of TAT-fusion proteins after lipid raft macropinocytosis. Nat Med 2004; 10:310–5.
[58] Fischer R, Fotin-Mleczek M, Hufnagel H, Brock R. Break on through to the other side-biophysics and cell biology shed light on cell-penetrating peptides. Chembiochem 2005;6:2126–42.
[59] Richard JP, Melikov K, Brooks H, Prevot P, Lebleu B, Chernomordik V. Cellular uptake of unconjugated TAT peptide involves clathrin-dependent endocytosis and heparan sulfate receptors. J Biol Chem 2005;280:15300–6.
[60] Murriel CL, Dowdy SF. Influence of protein transduction domains on intracellular delivery of macromolecules. Expert Opin Drug Deliv 2006;3:739–46.
[61] Vercauteren D, Vandenbroucke RE. The use of inhibitors to study endocytic pathways of gene carriers: optimization and pitfalls. Mol Ther 2010;18: 561–9.
[62] Langer R. Tissue engineering: a new field and its challenges. Pharm Res 1997; 14:840–1.
[63] Adams ML, Lavasanifar A, Kwon GS. Amphiphilic block copolymers for drug delivery. J Pharm Sci 2003;92:1343–55.
[64] Johnson NJ, Hanson LR, Frey 2nd WH. Trigeminal pathways deliver a low molecular weight drug from the nose to the brain and orofacial structures. Mol Pharm 2010;7:884–93.
[65] Kyrkanides S, Yang M, Tallents RH, Miller JN, Brouxhon SM, Olschowka JA. The trigeminal retrograde transfer pathway in the treatment of neurodegeneration. J Neuroimmunol 2009;209:139–42.